Planetary and Space Science 86 (2013) 117–129

Contents lists available at ScienceDirect

Planetary and Space Science

journal homepage: www.elsevier.com/locate/pss

Variability in ionospheric total electron content at Mars

Michael Mendillo [a], Clara Narvaez [a,*], Paul Withers [a], Majd Matta [a], Wlodek Kofman [b], Jeremie Mouginot [c]

[a] Center for Space Physics, Boston University, Boston, MA 02215, USA
[b] Institut de Planétologie et d'Astrophysique, Grenoble, France
[c] Department of Earth System Science, University of California, Irvine, CA, USA

ARTICLE INFO

Article history:
Received 26 February 2013
Received in revised form
12 August 2013
Accepted 13 August 2013
Available online 24 August 2013

Keywords:
Martian ionospheric variability

ABSTRACT

The Mars Express (MEX) mission includes a multi-purpose radio instrument called the Mars Advanced Radar for Subsurface and Ionospheric Sounding (MARSIS). When used in its ionospheric-penetrating subsurface sounder (SS) radar mode, a by-product of the MARSIS observations is the ray-path-integral of electron densities, called the total electron content (TEC). We have used the initial TEC database of approximately 1.2 million TEC values spanning the period June 2005 to September 2007 to study the basic characteristics of TEC morphology and variability. We find quantitative agreement between the TEC values measured and those computed from model simulations of global diurnal behavior. With the basic photo-chemistry of the martian ionosphere a well understood process, it is the departures from average conditions that need specification and modeling. Here we use MARSIS TEC to do this quantitatively. We explore the specification of variability using different ways to define it: standard deviations from sample averages versus departures from control curves.

For global studies, we computed the standard deviation (σ in %) of mean values of TEC (in TECU of 10^{15} e^-/m^2) sorted by latitude, longitude, solar zenith angle (SZA), local time, season, and locations with/without strong crustal magnetic fields (50 nT at 150 km). For daytime conditions (SZA $< 75^\circ$), the global average $\langle TEC \rangle$ is $\sim$6 TECU with $\sigma = \sim 20\%$, while for nighttime (SZA $> 105^\circ$) $\langle TEC \rangle$ is $\sim$0.3 TECU with $\sigma = \sim 75\%$. Daytime variability is enhanced in the latitude region 0–30°S, a pattern that needs validation by later observations before its source can be identified. Nighttime variability is noticeably larger in regions of strong crustal magnetic fields (**B**)—an effect noted by previous authors.

For regional studies, high resolution latitude patterns of variability in the southern hemisphere – within the longitude sector 150–210° of strong crustal-**B** values – were computed as percentage changes with respect to zonally-averaged patterns outside the region of interest. We present evidence for the first time of **B**-fields affecting the variability of the daytime ionosphere by small amounts ($\sim \pm 5\%$). Under nighttime conditions, the **B**-field associated variability is $\sim \pm 20\%$. The results also reveal an anti-correlation between daytime and nighttime variability ordered by the inclination angle (I) of the **B**-fields. TEC variability is greater as I approaches vertical at night, but higher during the day (by smaller amounts) where I approaches horizontal patterns.

1. Introduction

1.1. Background

The study of variability in any atmospheric parameter requires a sufficient number of observations from which statistical conclusions can be drawn. For the upper atmosphere and ionosphere of Mars, this was essentially impossible until the arrival of the Mars Global Surveyor (MGS) and the Mars Express (MEX) spacecraft at Mars. As summarized in Table 1 in Mendillo et al. (2003), twelve previous missions resulted in a total of 443 electron density profiles [$N_e(h)$] that provided samples of the ionosphere under broad ranges of solar activity, latitude, longitude, season and local time. Such samples spread unevenly over too many parameter-space conditions did not allow for a robust treatment of variability.

The radio occultation experiment on MGS produced approximately 5600 additional $N_e(h)$ profiles and thus the first opportunity to examine variability in systematic ways spanning the years 1998–2006. Initial attempts were conducted using periods of MGS observations near dawn (Mendillo et al., 2003), and by models tuned to dawn conditions (Martinis et al., 2003). Subsequent studies using MGS electron density profiles were conducted by

* Corresponding author. Tel.: +1 617 3532631; fax: +1 617 3536463.
E-mail address: cnarvaez@bu.edu (C. Narvaez).

0032-0633/$ - see front matter © 2013 Elsevier Ltd. All rights reserved.
http://dx.doi.org/10.1016/j.pss.2013.08.010

several groups to examine a broad spectrum of possible sources of variability. These included the influence of crustal magnetic fields (e.g., Krymskii et al., 2003; Withers et al., 2005), long-term changes in solar flux (e.g., Breus et al., 2004), short-term solar flares (e.g., Mendillo et al., 2006), solar-terminator geometry (Fox and Yeager, 2006) and sporadic meteor impacts (e.g., Withers et al., 2008; Pandya and Haider, 2012). A comprehensive review of daytime ionospheric variability appears in Withers (2009), and a thorough review of the overall status of observations and models for the martian ionosphere is presented in Haider et al. (2011).

The arrival of MEX at Mars in 2003 brought three types of radio measurements to observe the ionosphere: (a) the classic radio occultation method (Pätzold et al., 2005) for $N_e(h)$ profiles and (b) the Mars Advanced Radar for Subsurface and Ionospheric Sounding (MARSIS), an instrument used in two distinct modes. The Active Ionospheric Sounder (AIS) mode (Gurnett et al., 2005) uses radio signal reflections to determine the plasma frequencies for the portion of $N_e(h)$ profiles between the peak electron density (N_{max}) and the satellite height. The Subsurface Sounder (SS) mode is an ionospheric-penetrating radar (Safaeinili et al., 2003; Picardi et al., 2005) that measures radiowave group path delay and thus the integral of $N_e(h)$, called the total electron content (TEC). MEX is in a highly elliptical orbit and the conditions most suitable for each of the radio science experiments vary substantially from orbit to orbit. For MARSIS, both modes cannot be in operation simultaneously, and thus data coverage is far from uniform across the planet. Nevertheless, the initial set of MARSIS observations yielded approximately 1.4 million TEC values over the course of a full martian orbit (2005–2007). These data have been the subject of several papers dealing with analysis methods and initial scientific results (Safaeinili et al., 2007; Mouginot et al., 2008; Lillis et al., 2010). In this paper, we use the same 2005–2007 MARSIS TEC database to approach the topic of ionospheric variability over spatial scales ranging from global to regional.

1.2. The scientific roll of variability

As discussed in the review papers by Withers (2009) and Haider et al. (2011), and the many references they cite, the basic photo-chemical and dynamical processes that govern the martian ionosphere are well understood. Yet, to model the ionosphere on a given day, only the input of solar irradiance can be specified with any degree of confidence. If a model does not agree with data, adjustments can be made to a host of parameters and processes that are poorly constrained by observations. The differences between the baseline model and the parameter-tuned model are the sources of day-to-day variability that represent the ultimate challenge to the aeronomy of Mars.

Prior to the reviews cited of observational evidence for variability, Morel et al. (2004) presented a summary of potential origins of ionospheric variability, with emphasis on signatures to be found within TEC data. In Table 1 of their study, the sources of variability were characterized as either "Planetary" or "External." The ionospheric variability that arises from local sources includes, first and foremost, the unknown variability in the upper atmosphere's density and composition. These range from changes associated with gravity waves on time scales of less than an hour to tidal effects that range from sub-diurnal to seasonal. Atmospheric changes due to dust storms certainly cause ionospheric variability in comparison to periods of dust-free neutral atmospheres. Magnetic field anomalies can contribute to ionospheric variability by affecting the magnitudes and directions of plasma diffusion, the influence of electro-dynamic transport, and plasma instabilities. The external sources of variability described by Morel et al. (2004) include photon fluxes at EUV and X-ray wavelengths, direct solar wind impact, induced magnetic fields, the precipitation of energetic particles, meteoric input effects, and finally galactic cosmic rays. Each of these intrinsic or extrinsic mechanisms can be modeled, but with uncertainties that have few observational constraints. To take a single example, an ionospheric measurement said to portray the effects of energetic particle precipitation requires a baseline of 'normal variability' to judge if the single point observation is indeed unusual or within typical patterns.

The approach we adopt here is to address the topic of variability with the goal of specifying its temporal and spatial patterns. The MARSIS TEC data base is the largest consistent set of observations of the ionosphere at Mars. Yet, as will be described below, it is far from the ideal data source due to limitations arising from orbital and operational issues. The TEC parameter is a height-integrated observation that is dominated by the electron density near and above the altitude of peak density, and thus insensitive to small contributions that arise from meteoritic layers or ionization produced by cosmic rays. Yet, the fact that TEC is dominated by the peak density means that it is sensitive to the broad host of sources of variability described by Morel et al. (2004).

2. TEC as a diagnostic of ionospheric variability

While the physics of photo-production, chemical loss and plasma transport all have pronounced altitude dependences, the resultant total number of electrons in a column of unit cross section serves as a fundamental way to assess broad characteristics of an ionosphere. Changes in vertical profiles can have dramatic effects upon specific layers and yet not have an overall effect on integrated plasma content. Thus TEC data are well suited for studies of processes that result in a total increase or decrease in the ionosphere, as opposed to variability resulting from re-distributions in altitude of the existing plasma. Variability in TEC data are thus useful in assessing the impacts of day-to-day changes of solar irradiance, dynamics of the neutral atmosphere, and electrodynamical processes instigated by changes in the solar wind. The latter include a host of effects governed by the presence of magnetic fields: plasma produced by precipitating energetic particles, transport due to penetrating or in-situ generated electric fields ($\mathbf{E}$) via $\mathbf{E}\times\mathbf{B}$ drift, and plasma instabilities of various scale sizes.

In terrestrial aeronomy, TEC data (in units of 10^{16} el/m^2, called TECU) have played a fundamental role in observing ionospheric characteristics and variability (see Mendillo, 2006 for a review of early studies, and Bust and Mitchell, 2008 for current techniques). Today, vast networks of radio receivers are used to monitor the group path delay from the global positioning system (GPS) satellites. The resulting GPS-based TEC observations from thousands of stations collecting data minute-by-minute are the dominant mode of global observations of the Earth's ionosphere. This is particularly important when geomagnetic storms occur and traditional groundbased radio-reflection observing methods ("ionosondes") are less able to cope with small scale irregularities that spread the reflected signal in frequency and phase, or when plasma gradients produce oblique echoes from non-vertical directions.

When both TEC values and the peak electron density of the ionosphere (N_{max}) are available at Earth, it is seen that they are highly correlated, with an overall average correlation coefficient of $\sim$0.9 (Fox et al., 1991). The ratio (TEC/N_{max}) is called the equivalent slab thickness (τ) of the ionosphere, the effective breadth of a plasma layer having constant peak density that accounts for the TEC. Because of the high correlation between TEC and N_{max}, the variability of slab thickness is lower than either, and thus τ tends to highlight the differences between them. Given this behavior, models of slab thickness were long used when applications

required the parameter not measured (N_{max} or TEC) to be obtained from one that was (Fox et al., 1991). Scientifically, the main use of slab thickness has been to estimate the scale height of the upper atmosphere and therefore its neutral temperature (Titheridge, 1973).

The first studies of the TEC at Mars were made possible by simply integrating the initial sets of $N_e(h)$ profiles that came from the MGS mission (Mendillo et al., 2004). Using fixed altitude limits (100 to 200 km) for 209 profiles obtained in the 1998–2000 period, the resultant TEC values (in units of 10^{15} e^-/m^2, adopted as martian TECU hereafter) were shown to be $\sim 4.2 \pm 10\%$ for dawn conditions (03-04 LT) at high latitudes ($\sim$68N). Adding approximations for the TEC below 100 km (1 TECU) and above 200 km (2 TECU) to maintain a factor of two ratio for TEC above and below the height of peak density (Wright, 1960) led to an estimated mean TEC of $\sim$7 TECU. For the slab thickness parameter (easily formed since the full $N_e(h)$ profiles were available), τ had an average value of $\sim 53 \pm 6$ km. This slightly higher variability (11.5%) than found for TEC suggested that changes in shape of the ionosphere were linked more directly to its peak density (Mendillo et al., 2004).

Similar estimates can be made using models. For example, for noontime (sub-solar-point) conditions and the 100–200 km altitude range, the Mars ionosphere model described in Martinis et al. (2003) was run using extremes of solar activity (solar max vs. solar min) at the extremes of the martian orbit (perihelion and aphelion points). The results showed that for the 100–200 km altitude range, the daytime maximum TEC values could vary between 7 and 14 TECU (Mendillo et al., 2004). Adding the prior estimates for the contributions to observed TEC that come from regions below 100 km and above 200 km lead to peak TEC values of 10 to 17 TECU for solar minimum and solar maximum conditions, respectively. Prior to the arrival of Mars Express, there were simply no ways to validate such estimates using observed TEC.

With the availability of the MARSIS observations on MEX, the first comprehensive set of TEC data became available for analysis. The key findings from these initial studies led to an impressive set of morphology patterns for TEC at Mars:

(1) TEC is dominated by the photo-chemical layers (M1 at $\sim$110 km and M2 at $\sim$130 km) and thus TEC values show a strong solar zenith angle (SZA) dependence (Safaeinili et al., 2007; confirmed by Lillis et al., 2010). For the sub-solar point (SZA$=0^\circ$), the TEC approaches 10 TECU for solar minimum conditions, in excellent agreement with the sub-solar point estimate made from modeling solar minimum conditions, as described above.
(2) For changing solar flux conditions, the relationship between TEC and solar flux showed the typical Chapman-type power law pattern [TEC$\sim$(solar flux)$^{0.5}$], with the exponent being 0.54 when measured solar EUV is used and 0.44 when the radio flux proxy (F10.7 index) is used (Lillis et al., 2010).
(3) For nighttime conditions (SZA $> 100^\circ$), the TEC has low values of 0.2 to 0.3 TECU and enhancements over the global mean are seen in regions where crustal magnetic fields (**B**) with vertical inclination angles occur (Safaeinili et al., 2007).
(4) When the strong SZA dependence of TEC is removed, and residuals are compared with seasonal and dust storm periods on Mars, no clear patterns emerged (Lillis et al., 2010). TEC increases were seen in residuals when a solar energetic particle (SEP) event occurred (Lillis et al., 2010).

The results summarized above give the initial picture of variability patterns for TEC at Mars. Some of the conclusions are based on sub-sets of the MARSIS database (e.g., the nighttime analysis utilized 16 of the 26 months, and the correlation between higher TEC with **B**-field inclination angle utilized a single orbit). Also, enhancements in TEC were emphasized in all cases when, of course, variability involves both positive and negative deviations about a mean.

In the most recent study of MARSIS TEC data (Cartacci et al., 2013), the database was expanded to include observations made during four additional years (2008–2011). Cartacci et al. (2013) also described an independent analysis method of deriving TEC values from the MARSIS observations (called the contrast method) —a technique they portrayed as best suited for nighttime data "with the caveat that they can be affected by an overestimate of up to 10%." Working with 4600 MEX/MARSIS orbits from 2006 to 2011, Cartacci et al. (2013) conducted the most systematic analysis of TEC nighttime variability to date. For each orbit, the nighttime portions (defined as solar zenith angles greater than 90°) were fit with 10th order polynomials, with departures from the fits used to define ΔTEC(%). Their overall results for nighttime TEC variability defined in this way were: (a) ΔTEC(%) values were mostly between $\pm$20%, (b) ΔTEC(%) was higher in regions where crustal magnetic fields were more vertical, and (c) there was no prominent dependence of the ΔTEC(%) patterns on the magnitudes of the crustal **B**-fields.

We offer in this paper alternate ways to characterize TEC variability at Mars. We use the initial two-year MARSIS TEC data base derived using the analysis method of Mouginot et al. (2008) for two reasons: (a) The nighttime data analyzed by Cartacci et al. (2013) using their independent protocol resulted in TEC values that "generally agree and display similar fluctuations and trends" as found using the Mouginot et al. method. This is an important validation advancement for the lowest values of TEC—lessening concerns about their use in a large statistical study, and (b) We wanted to study TEC variability under daytime conditions. The 2005–07 data set had daytime values that could not be used if derived by the contrast method, as explained in Cartacci et al. (2013). Our analysis approach is also guided by methods used in terrestrial aeronomy that do not rely on the use of solar zenith angle (SZA) as the most important ordering parameter. A solar zenith angle is, of course, a key parameter in any photo-chemical processes, but it cannot differentiate between the components of SZA determined by latitude and local time—and thus we devote attention to those types of spatial and temporal parameterizations. We characterize variability in two ways: for global studies we bin TEC values by various parameters to form averages and standard deviations from the observed values; for regional studies we form control curves of parameters outside the regions of interest and compute departures from them. Numerical results from such an approach differ from those obtained in Cartacci et al. (2013) where TEC variability was quantified as departures from a 10th order polynomical fit to data taken along each sub-orbital track. That approach is certainly useful for determining variability along smooth latitude/longitude patterns. When structure is present, however, a high-order control curve might actually reduce quantifiable variability by allowing the control curve to have, in itself, significant departures from a smooth ionosphere. With these types of issues in mind, we now describe our alternate ways to define ionospheric variability, to characterize both its daytime and nighttime patterns, and to portray the results over spatial scales ranging from planet-wide to regional.

3. Global patterns: Analysis methods

We have taken the $\sim$1.4 million TEC values obtained from June 2005 to September 2007 from the MARSIS data archive site (ftp://www.psa.esac.esa.int/pub/mirror/MARS-EXPRESS/MARSIS/), and selected those with a "data-quality" index$=1$ for analysis. The

lower quality data not examined tended to come mostly from early times in the mission. The final database, nevertheless, remained large, with ~1.2 million values used. With a goal of characterizing large-scale variability, we did not use the MARSIS TEC data at their highest possible spatial and temporal resolutions ($<1^\circ$, <1 s). For global-scale analyses we binned data into latitude boxes of 5° and 1-h local time segments. In later plots, we also use longitude boxes of 15° and latitude bins of 2° for higher resolution of patterns near crustal **B**-fields. Average values were computed for each bin, and also the 1-sigma standard deviations (σ) about the mean. We quote all total electron content values in TEC-units (TECU, as defined above), and standard deviations in percent, σ(TEC, %).

The MARSIS radar operates with frequencies between 1.3 and 5.5 MHz, and thus for the radio signal to penetrate the ionosphere the local plasma frequency must be less than 5.5 MHz. This corresponds to a peak electron density of $\sim 4 \times 10^{11}$ e$^-$/m^3 for daytime conditions which – for a slab thickness of ~53 km (see above) – would yield a maximum total electron content of 8–10 TECU. This matches the highest values found in this data set, and thus we do not anticipate an under-estimation of the daytime TEC values due to sampling limitations for this period in the solar cycle. For the lower limit of 1.3 MHz, corresponding to the plasma frequency for a peak electron density of $\sim 0.2 \times 10^{11}$ e$^-$/m^3, the minimum TEC detectable (assuming a diurnally-constant slab thickness parameter) would be ~0.4 TECU, consistent with the ~0.3 TECU minima reported in all previous MARSIS studies for nighttime conditions.

Operationally, the MARSIS measurement sensitivities depend on the frequencies being used, and these have been described in Mouginot et al. (2008). Quoting from their Table 1, their weighted-mean sensitivity averages were 0.35 TECU for daytime and 0.15 TECU for nighttime values. These imply robust TEC values for daytime conditions, with confidence limits within a factor of two for nighttime conditions. The accuracy of any measurement will always depend to some extent upon its magnitude, and thus the percentage changes of low nighttime values of TEC will have less statistical certainty than the daytime ones. In spite of these lower reliability levels for nighttime observations, virtually all prior results referenced above have dealt with the use of nighttime TEC data. Here we extend analyses of variability by using all available daytime data.

3.1. Seasonal characteristics for TEC and its variability: Diurnal patterns

We divided the MARSIS TEC data into three orbital longitude sectors (Ls) corresponding to (a) summer in the northern hemisphere, Ls=30–150, (b) winter in the northern hemisphere, Ls=210–330, and (c) equinox, taken as the sum of the northern hemisphere spring and fall sectors, Ls=330–30 plus Ls=150–210. To display the results we use a global coordinate system of latitude vs. local time. This neglects any possible effects ordered by longitude which, as will be shown below, seems a reasonable first approximation.

Using the latitude versus local time format, the results for the mean values in absolute units (TECU) are given in the top three panels of Fig. 1. One can see that coverage in local times is far from complete (particularly from midnight to dawn), even when one-third of the total data base is used for each season. Nevertheless, one can see the essential features of each season. At high latitudes under solstice conditions in each hemisphere, panels (a) and (b), sunlight is present at all local times in local summer and TEC has a relatively small diurnal variation (~4–7 TECU). For the winter solstice conditions in each hemisphere, the absence of sunlight at high latitudes leads to no photo-chemically produced plasma, and thus the low values observed (rarely exceeding 1 TECU) must result from horizontal transport from other locations, or from energetic particle precipitation effects. In panel (b), the only solstice period with good coverage at mid-day, the peak TEC values (~10 TECU) occur at local noon, in accordance with basic photo-chemistry. For the sunset sector at mid-latitudes, the signature of an ionosphere strongly controlled by solar zenith angle is evidenced by the severe gradient in local time to low nighttime values (~1 TECU). In fact, the slanted terminator, aligned from early to late local times with latitude (north to south) is clearly apparent in panel (b). Finally, the equinox results in panel (c) exhibit portions of a symmetrical pattern in latitude and local time. All of these results are in accord with the solar-zenith-analysis in Lillis et al. (2010), re-portrayed here using the planet's spatial (i.e., latitude) and diurnal (i.e., local time) characteristics.

To assess TEC variability for each season, the standard deviations σ(%) about the mean values are shown in the lower three panels of Fig. 1. The basic pattern is that variability (as characterized by σ) is inversely proportional to the magnitude of TEC. For example, under mid-day conditions, variability in electron content is typically 10–20%, while variability in the post-sunset and nighttime TEC values is considerably higher (~50–100%). This factor of five difference in variability between daytime and nighttime is in marked contrast to F2-layer on Earth where its peak density and TEC have diurnal variabilities that differ by less than a factor of two, typically ~20% (day) and ~35% (night) (Forbes et al., 2000; Rishbeth and Mendillo, 2001).

3.2. Spatial characteristics of TEC variability: Latitude and longitude patterns versus solar zenith angle conditions

The results from the lower three panels in Fig. 1 show that overall variability has a diurnal component, with nighttime σ(%) values being greater than daytime ones. Statistically, this is to be expected in that small ΔTEC changes upon low nighttime TEC values result in larger percentage changes than would occur for the same ΔTEC under daytime conditions. The initial study of Safaeinili et al. (2007) showed that ionospheric behavior under nighttime conditions can also be affected by the spatial location of the observations (i.e., near or far from crustal magnetic fields). To explore the overall latitude–longitude dependence of variability under daytime and nighttime conditions, we now turn to a series of plots that probe σ(%) under two broad sets of solar illumination: SZA $< 75^\circ$ ("daytime") and SZA $> 105^\circ$ ("nighttime"). We avoid the dawn and dusk periods since they are more complex transitional domains, as shown graphically in Fig. 1 and as discussed in Safaeinili et al. (2007). It must be recognized that use of SZAs introduces possible data-binning biases due to the different ways a large SZA can occur. SZAs prior to sunrise and after sunset are, of course, all greater than 90°. Near dawn and dusk, however, SZAs can be close to 90°, but that can also occur at local noon at polar latitudes, as well as during many daytime hours at high latitudes during winter solstice conditions. It is for these reasons that we used latitude and local time in Fig. 1, and now turn to latitude–longitude plots for fixed ranges of solar zenith angles.

Fig. 2 shows the global variability patterns for σ(TEC, %) when the MARSIS data are sorted by SZA, as defined above—with daytime results (top) and nighttime results (bottom). The daytime coverage is adequate, except in the northern hemisphere latitude range of 35–65°N. Note also that the data at north and south polar latitudes come from their respective solstice seasons, and that there are no significant differences in the σ(TEC, %) between the two solstices. The major feature seen in Fig. 2(a) is that daytime variability at virtually all longitudes is higher in the latitude span 0–30°S. This conclusion is fairly robust in that data coverage spans the equator, but the variability is clearly more pronounced at low

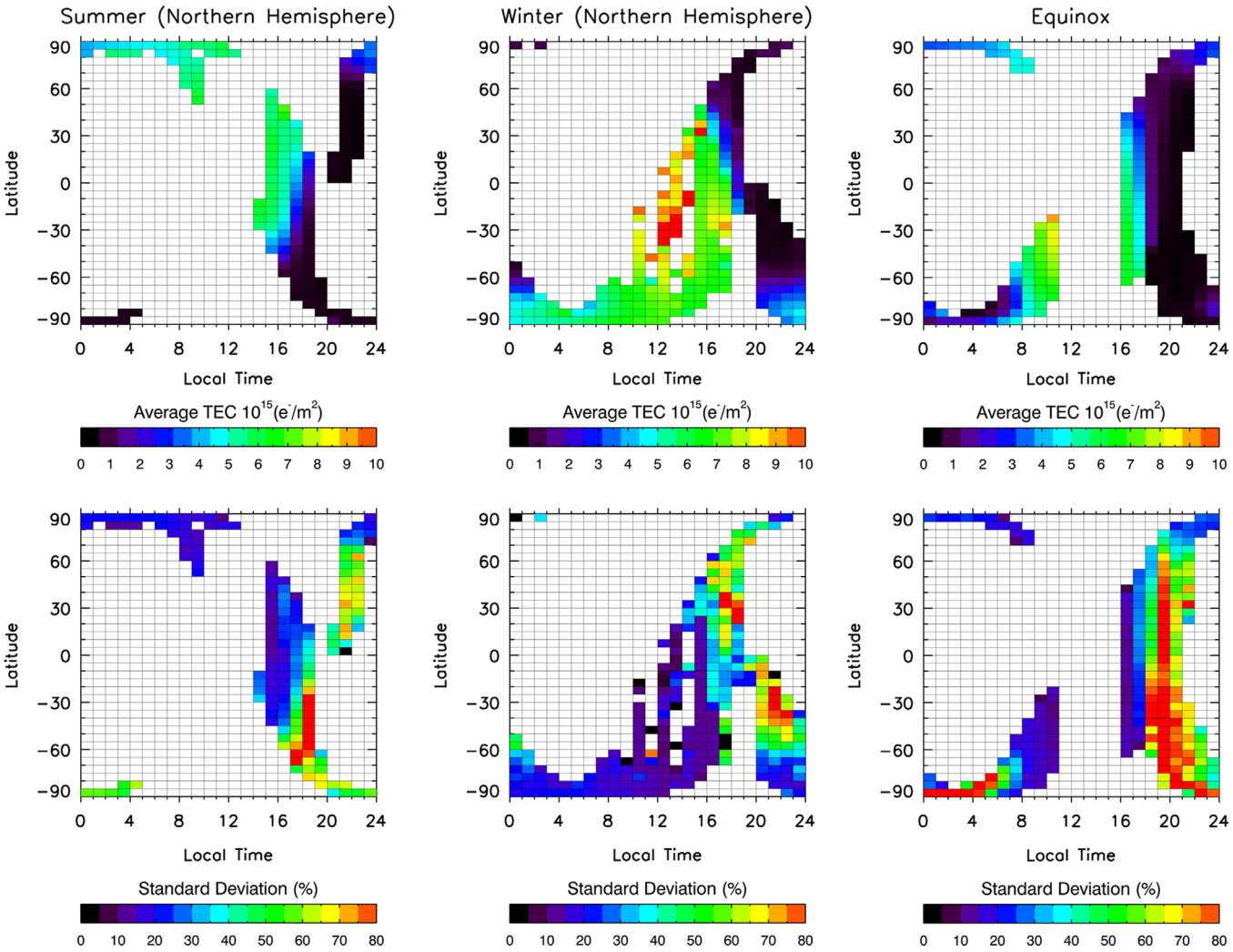

Fig. 1. Global distribution of total electron content (TEC) of Mars as a function of season, latitude and local time. The spatial resolution is 5° in latitude and the time resolution is 1 h. In the top three panels, the mean values of TEC for northern summer, northern winter and equinox periods are displayed using the color bar in TEC-units (defined as 10^{15} e^-/m^2). In the bottom three panel, ionospheric variability in the same three data sets is portrayed using the standard deviation σ(%) about the mean (see text). Data numbers averaged per bin range from 2 to 16,858.

latitudes in the southern hemisphere. It is tempting to associate the 0–30° South latitude pattern of enhanced variability in Fig. 2 with the zone of crustal magnetic fields that span the same latitude–longitude range (see Fig. 3(a)). Yet, there are longitudes with stronger crustal **B**-fields (135–270°E) that extend from the equator to the southern pole—and there are no σ(TEC, %) maxima of equal magnitude in those regions of Fig. 2(a). If this low-latitude variability is not related to processes dependent upon magnetic fields, other possibilities include some type of neutral atmosphere variability. For example, low-latitude zones of small-scale (<10 km) wave activity versus longitude were discussed in detail by Creasey and Forbes (2006) using MGS radio occultation observations of the lower atmosphere (ground to ~40 km). Their results did not show a pronounced hemispheric asymmetry at low latitudes, referring to wave activity as "predominantly in the Martian tropics." The Creasey and Forbes (2006) results, nevertheless, point to the important effects that variability in the neutral atmosphere might have upon the ionosphere, assuming that upward propagation of low altitude gravity waves are not inhibited or filtered out by winds at higher altitudes.

A second feature apparent in the daytime results in Fig. 2(a) is the somewhat periodic structure in longitude of the low latitude variability. There are about twelve such bands of enhanced TEC variability spanning the planet, and this suggests a sampling bias. Specifically, we found that they do tend to be associated with MARSIS passes having higher solar zenith angles (60–75°). As shown in Fig. 1, TEC variability increases dramatically with SZA, and thus post-sunrise and pre-sunset data (while considered daytime) would have higher variabilities. Yet, removal of these 60–75° SZA data did not fully remove the variability enhancements near 30°S. Analysis of the post-2007 MARSIS data sets will be needed to determine if a band of enhanced daytime TEC variability actually exists at low latitudes.

The global pattern for σ(TEC, %) for nighttime periods is presented in the lower panel of Fig. 2. Spatial coverage is more complete under these high solar zenith angle conditions, with only the ~55–90°N region showing appreciable gaps in observations. Note that the color-coding has a factor of three difference between the two panels, i.e., red is ~25% during daytime (top) and ~75% at night (bottom). As expected from the discussions above, the nighttime variability has more of a dynamic range than daytime variability over the entire planet. Within this context, it is nevertheless quite clear that the global maxima for ionospheric variability occur in precisely the latitude–longitude range of the strongest **B**-fields (30–90°S, 135–225°E) shown in Fig. 3. This pattern extends the results of Safaeinili et al. (2007) where only TEC enhancements were attributed to this region, to all forms of TEC variability captured in a statistical sample. In the larger

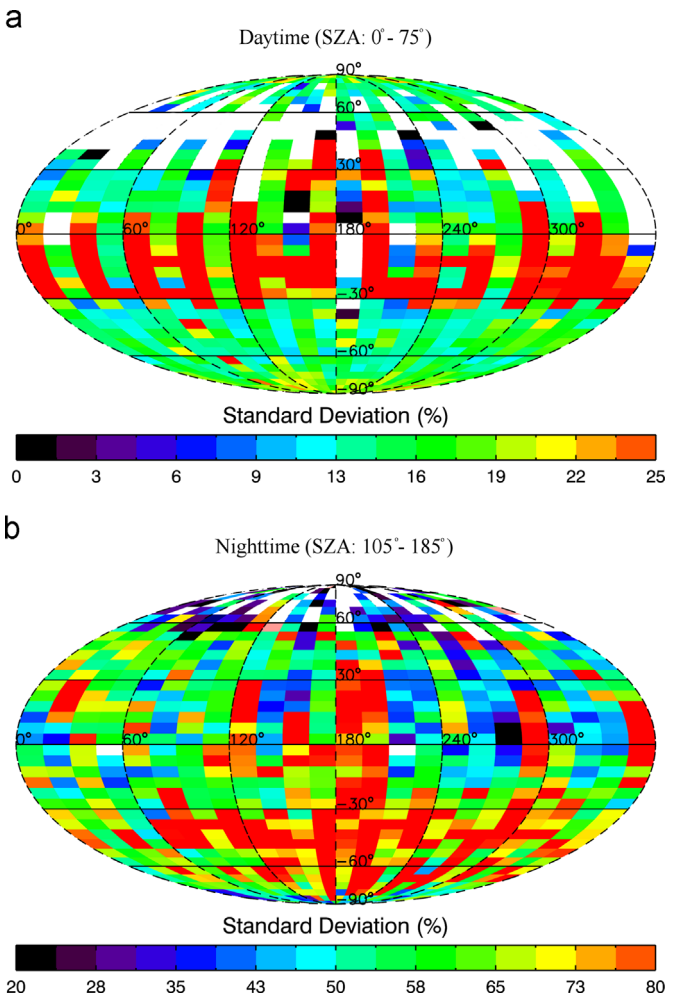

Fig. 2. The global distribution of ionospheric variability, as defined by the standard deviation, in percent, of TEC means computed using bins of 5° in latitude and 15° in longitude. Panel (a) is for daytime conditions defined as SZA < 75° and panel (b) is for nighttime conditions defined as SZA > 105°. Note the different scales for σ(TEC, %) used for each panel.

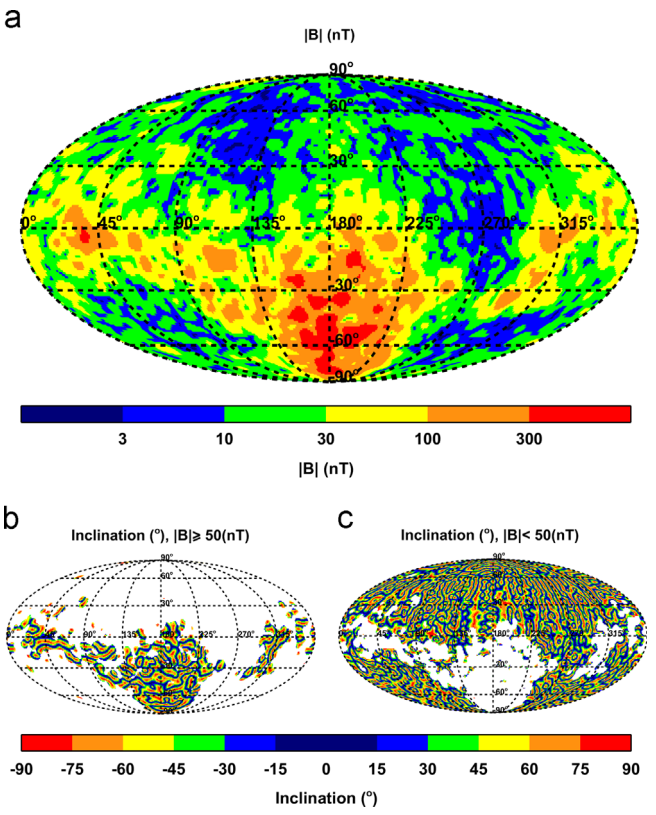

Fig. 3. (a) The distribution of magnetic field strength (|**B**|) at Mars at an altitude of 150 km on a grid of latitude and longitude, taken from the model of Arkani-Hamed (2004). The zone of peak **B**-field magnitude in the southern hemisphere is centered on the meridian at 180°E. (b) The global distribution of magnetic field inclination angles (I) for regions where the ambient **B**-field is greater than 50 nT, and in (c) for regions where the **B**-fields are less than 50 nT.

nighttime data set used by Cartacci et al. (2013), their Fig. 8 shows this to be a consistent pattern over the entire 2005–2010 period of MARSIS TEC observations.

While nighttime TEC variability is most prominent in the crustal-**B** regions, it important to realize that those regions span a relatively limited portion of the martian globe. In Fig. 4 we show the longitude-averaged profile of TEC magnitude versus latitude for both daytime and nighttime conditions (left panel). Their corresponding 1-sigma variabilities are given in the right panel. In this format, there are many thousands of TEC values within most of the latitude bins but, in areas of sparse coverage, there can be as few as 500 (or less) TEC values in the average. Dashed lines are used to show results for those less reliable latitudes. For the daytime results in the left panel, we show latitude profiles for two cases: broad daytime coverage (0–75° SZA in the red curve) and restricted daytime coverage (0–60° SZA) with the black curve. Examination of the 0–75° SZA curve shows that there is no significant latitude dependence upon the absolute values of such a zonally-average TEC for full daytime conditions, with a mean value of 5.8 TECU. For the more restricted daytime curve (0–60° SZA in black) there is some indication of enhanced TEC values near ±30° latitudes; the overall mean for this case is 6.3 TECU. For nighttime conditions, the latitude profile is essentially flat with an average value of 0.3 TECU. Thus there are no enhancements to note in zonally-averaged patterns that arise from the TEC in crustal-**B** region longitudes in the southern hemisphere. It is important to recall that seasonal effects upon latitude patterns are suppressed in a plot that uses observed TEC from all seasons—sorted only by solar-zenith angle. Also, data gaps at pre-noon local times (see Fig. 1) result in most of the "daytime" values coming from the afternoon sector. The average values quoted (~6 TECU day and ~0.3 TECU night) are consistent with the Lillis et al. (2010) results for approximately 60° SZA (daytime) and 120° SZA (nighttime).

The right panel in Fig. 4 gives the variability results. For daytime conditions, there are again two cases for SZAs, associated with their corresponding curves in the left panel. For the full daytime plot (red), σ(TEC, %) has an average value of 20.2%, with some latitude structure. Specifically, the variability is ~15% at most latitudes—except for the latitude band from the equator to ~30°S where it is about double that value. This corresponds to the same high-variability feature that appears at all longitudes in Fig. 2. For the more restrictive daytime results (black curve), the σ(TEC, %) mean of ~15% is more representative of all latitudes, with only a slight enhancement again at 30°S.

For nighttime conditions in Fig. 4, TEC variability shows considerably higher values, as expected from Fig. 2(b). The average over all latitudes is ~75%. The mean of the northern hemisphere is ~66%, with a structured pattern, but one that generally decreases from equator to pole. For the southern hemisphere, the mean variability is ~81%, with the highest values and most structured pattern occurring at latitudes near 60° South where the crustal-**B** fields are strongest (Fig. 3a). A closer examination of crustal-**B** region patterns is done in the next section. To summarize the global results in Fig. 4, the overall variability of TEC for the martian

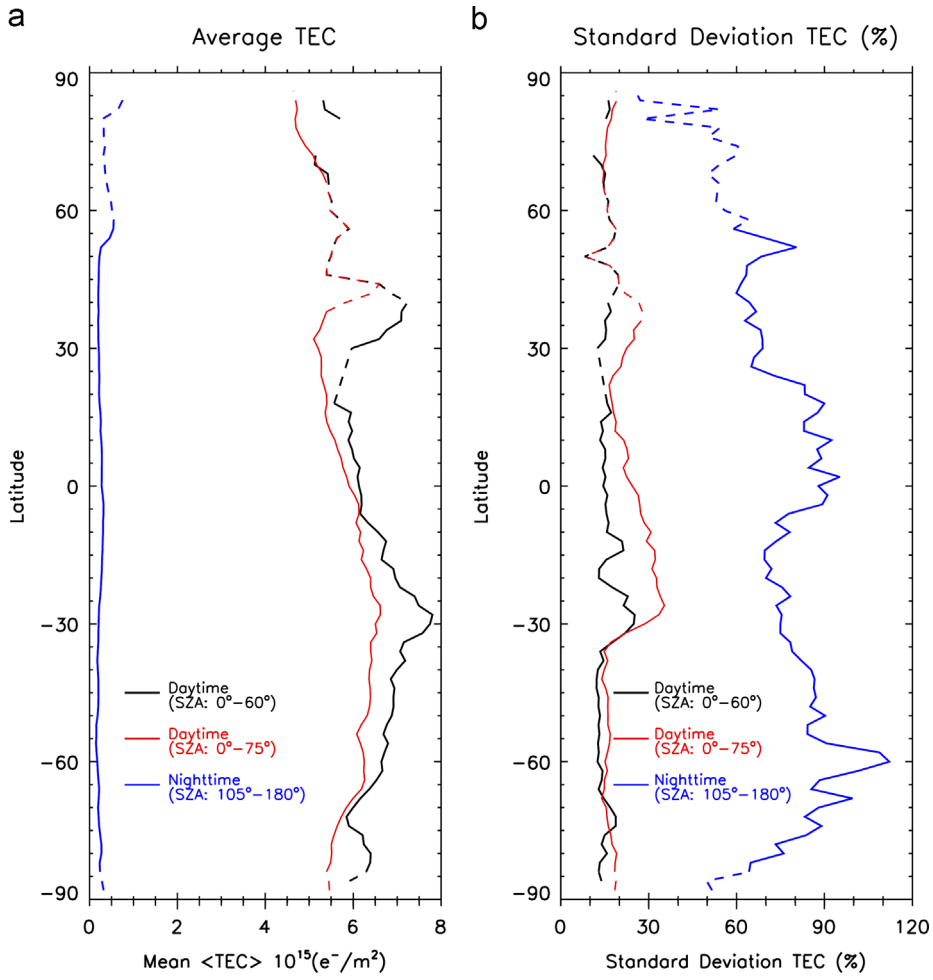

Fig. 4. Zonally-averaged latitude profiles of TEC and its variability using two characterizations of daytime conditions (SZA < 75° red; SZA < 60° black) and a single nighttime conditions (SZA > 105°). Panel (a) gives TEC in absolute TEC-units, and panel (b) gives their 1-sigma variability in percent. Latitude resolution is 2°, in contrast to the 5° resolution used in previous figures. Regions of sparse data coverage shown using dashed lines (see text).

ionosphere is 15–20% daytime, 60–100% nighttime. This pertains to periods of low solar activity and minimal dust storms, and therefore constitutes a base-level definition of ionospheric variability from which periods of disturbance can be gauged.

4. Regional patterns of ionospheric variability

4.1. Background

The initial analysis of MARSIS TEC observations (Safaeinili et al., 2007) revealed an association between nighttime enhancements in electron contents with regions of high inclination angle (I) of crustal magnetic fields (**B**), where $I=90^\circ$ corresponds to a vertical-**B** and $I=0^\circ$ to a horizontal field. As reviewed by Safaeinili et al. (2007), this had been a much-anticipated finding once the crustal-**B** fields were discovered (Acuña et al., 1998; Connerney et al., 2001; Krymskii et al., 2004; Nagy et al., 2004; Gurnett et al., 2005; Duru et al., 2006). Identifying unusual patterns of the ionosphere embedded within regions of crustal fields has been achieved in several ways (see Haider et al., 2011 and Zou et al., 2010 for comprehensive reviews of the topic). Using MGS radio occultation data to study unusual $N_e(h)$ profiles under sunlit conditions, Withers et al. (2005) showed that both electron density enhancements and depletions occurred in regions of crustal-**B**. In addition to precipitation-induced enhancements, plasma instability processes were also mentioned as a possible source of both the enhancements and depletions. Withers et al. (2005) did not, however, integrate the MGS $N_e(h)$ profiles to see what signatures the "bumps and bite-outs" might have on the TEC magnitudes in regions of crustal-**B**. On the MEX satellite, the MARSIS topside-ionosonde (AIS) has been used to identify nighttime "patchy" regions of enhanced densities located in the vicinity of crustal-**B** fields. These were detected via the effects they produce ("oblique echoes") upon non-vertical radiowave reflections from **B**-field-aligned plasma (Němec et al., 2010, 2011). Here we will use the MARSIS TEC observations directly to explore such effects—contrasting regions with and without strong magnetic fields.

On Earth, ionospheric enhancements have long been known to occur in regions of high magnetic field inclination angle. Along the auroral oval, high energy (> kev) particles penetrate to the E-region to cause both visible aurora and plasma enhancements. Also on the nightside, very-low-energy (10 s of ev) precipitating particles from the magnetospheric plasma sheet ionize thermospheric neutrals to create the poleward plasma wall of the ionosphere's sub-auroral F-layer trough (Mendillo and Chacko, 1977), as well as the sub-visual diffuse aurora at 6300 Å. On the dayside, low-energy (100 s of ev) magnetosheath particles precipitate down converging magnetic field lines within the cusps to produces high-latitude ionospheric $N_e(h)$ enhancements (Chacko and Mendillo, 1977). All of these enhancement effects are readily observed in GPS TEC observations that integrate over the full

ionosphere. These high-inclination angle processes occur over extended latitude and longitude regions due to the global nature of the geomagnetic field.

At equatorial latitudes on Earth, where the geomagnetic field is essentially horizontal, the solar-produced ionosphere also experiences significant modifications related to the geometry of the magnetic field. Local electric fields, winds and instability mechanisms produce both positive and negative distortions of the ambient ionosphere via processes that depend on the spatial patterns of small inclination angles. Again, GPS TEC observations at low latitudes show dramatic increases and depletions due to such effects. At their largest scale, these low latitude effects result in the so-called equatorial fountain effect and the equatorial spread-F plumes (Rishbeth and Garriott, 1969; Schunk and Nagy, 2009; Kelley, 2009) that span 15–20° North and South about the geomagnetic equator at all longitudes.

The situation is completely different at Mars. The separations between cusp and equatorial **B**-patterns occur within 10–100 s of kilometers (rather than the 1000 s of kilometers seen on Earth), and thus one must use with caution such phrases as "cusp-like" and "equatorial-like." This is due to the fact that, over the small spatial scales of the crustal-**B**-field patterns, coupling between adjacent field morphologies probably occurs, even in ionospheric layers where photo-chemistry is dominant. For the TEC parameter, in particular, where 2/3rd of the integrated content comes from regions above the height of peak density, transport becomes important at topside heights near ~170 km (Mendillo et al., 2011). Moreover, just because a region has a measureable **B**-field, it is not always obvious that it is strong enough to exert an influence on ionospheric processes. In Fig. 16 (panel d) of Mendillo et al. (2011), it is shown that vast regions of Mars' ionosphere can occur under high-beta conditions, i.e., with ionospheric pressure greater than magnetic pressure, thus minimizing the influence of the **B**-fields present.

4.2. *Disturbed and quiescent zones within the martian ionosphere*

The MARSIS TEC data are well-suited to explore the complexities of ionospheric behavior within large-scale regions of weak **B**-fields versus those found within spatially-confined regions of strong **B**-fields. The few prior studies using the same two-year MARSIS TEC database have dealt with a relatively small number of cases, as mentioned above. The most recent investigation by Cartacci et al. (2013) used five years of nighttime data for a very comprehensive study of nighttime crustal-**B** effects, also summarized above. Here, where our focus has been on daytime effects as well as nighttime, we use the original two-year dataset to identify persistent, statistically-significant links between TEC perturbation morphologies and magnetic field inclination patterns. To do so, we increased latitude resolution from 5° to 2°, and conducted identical analyses of two latitude–longitude sectors on Mars with contrasting **B**-field characteristics. These are: (1) the latitude span 30–90° South at longitudes 150–210°E (called the high-**B** region) and (2) the latitude span 30–90° North at longitudes 240–300°E (called the low-**B** region). As seen from Fig. 3 (panels (b) and (c)), and from the discussion above, we used 50 nT as the dividing point between high and low **B** values to show where the ionosphere might be affected by processes that depend on inclination angle (I). The choice of 50 nT as a reference magnitude is consistent with the MHD modeling studies of the threshold effects that various **B**-field characteristics would have at Mars—studies done prior to their actual discovery (Shinagawa and Cravens, 1989).

The magnetic field topology at Mars has two components: (a) localized intrinsic fields ("crustal") and (b) omni-present, but variable, induced fields ("draped") dependent upon the magnitude and direction of the interplanetary magnetic field (IMF) carried by the solar wind, with penetration depth also a function of the solar wind's dynamic pressure. In the high-**B** sector defined above, a series of mini-dipole patterns exist with a full range in inclination angles present (similar to a chain of sunspot **B**-fields). Examples of magnetic field line morphologies within the martian ionosphere appear in Withers et al. (2005) and Mendillo and Withers (2008), with a useful schematic of **B**-lines versus latitude and height in Zou et al. (2010). For the draped fields, the topology is basically horizontal under daytime conditions, with a transformation to more radial directions beyond the dawn–dusk terminator. In our analysis we do not separate these in any fundamental way, but rather search for TEC patterns related to the local-time-invariant **B**-field model of Arkani-Hamed (2004).

Fig. 5 gives the patterns of inclination angle for the two regional (high-**B**, low-**B**) sectors. Note that we assign the same color-codes to the same magnitudes of the inclination angle, e.g., red to $I = \pm 90°$ because, from an ionospheric physics perspective, it does not matter if the field points up or down. In panel (a) for $\mathbf{B} > 50$ nT, there is only a zonal pattern for inclination angles, while in panel (b) for $\mathbf{B} < 50$ nT, there are both zonal and meridional patterns. Thus, averaging over longitude preserves the crustal-**B** characteristics where it matters (in the southern hemisphere), while it mixes inconsistent I-contours where it does not matter (in the northern hemisphere).

As can be seen from Fig. 1, the data coverage for the control sector (low-**B**) is less complete during daytime in the 30–50°N latitude range, and in the 60–90°N latitude range at night. Fortunately, this is not the case in the high-**B** sector. We formed

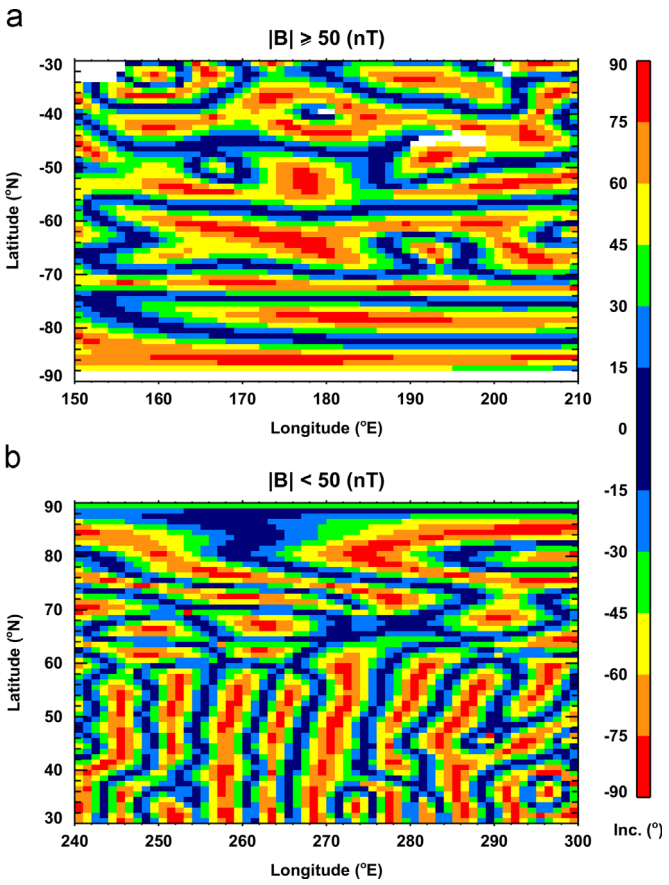

Fig. 5. The latitude–longitude characteristics of the magnetic field's inclination angle (I) in two widely separated regions on Mars used in case studies of ionospheric variability. In (a) the high-**B** region in the southern hemisphere is between longitudes 150–210° East and in (b) the low-**B** region in the northern hemisphere is between longitudes 240–300° East. In both panels, the latitude span is 30–90° in each hemisphere. See text.

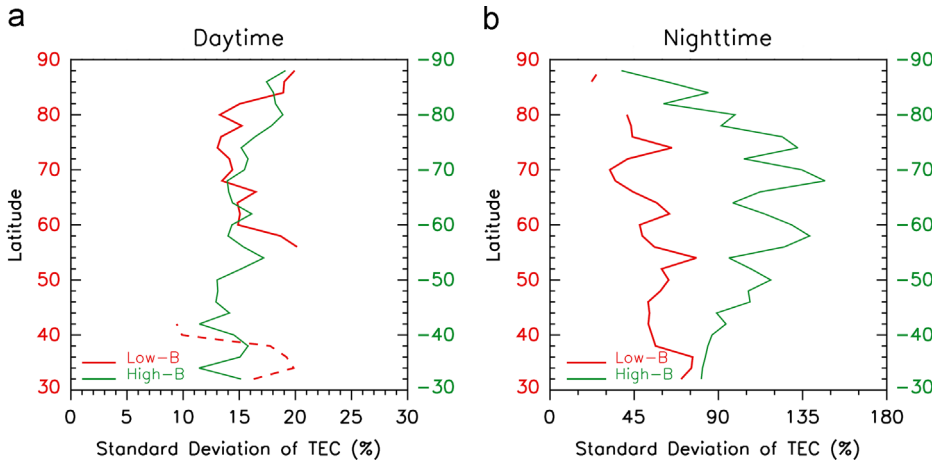

Fig. 6. Latitude profiles of the standard deviations, σ(%), of mean TEC values for the high-**B** and low-**B** regions. Latitude resolution is 2°. (a) Daytime results are given by the solid green line (right axis) for the high-**B** region and by the solid red line (left axis) for the low-**B** region. (b) Nighttime results using the same format. Dashed line segments refer to results where data coverage is sparse, and gaps in line segments refer to regions where no data exist (see text).

the average TEC versus latitude profiles for each region together with their standard deviations. Fig. 6 presents the variability patterns for the two regions. For daytime conditions, the low-**B** and high-**B** sections have consistent standard deviations of about 15–18%. For nighttime conditions, there is a clear separation between the variability characteristics of the two regions, with the high-**B** variability magnitudes ($>$ 90%) more than double those in the low-**B** pattern ($\sim$45%). There is also considerably more structure with latitude in the high-**B** sector.

To explore further the details of variability within the high-**B** sector, we now turn to a comparison of TEC observations made only in the southern hemisphere. We switch from using standard deviations about mean behavior to percentage changes from a control curve. To form a control curve, we computed a zonal average for each 2° latitude bin within the southern hemisphere, but excluding data from the high-**B** longitude sector. The resultant ΔTEC (%) versus latitude patterns for the high-**B** sector appear in Fig. 7. For the daytime conditions in panel (a), ΔTEC (%) averages to about +5% (with structure at the $\pm$5% level). Thus, the ionosphere is slightly enhanced during daytime hours in the southern hemisphere's high-**B** sector with respect to the same latitudes at other longitudes. For nighttime conditions, a different pattern emerges. Panel (b) shows ΔTEC (%) to have a latitude average near zero, meaning that the TEC magnitudes in the high-**B** sector are, on average, equal to those at other longitudes. However, there is considerably more spatial structure versus latitude in the high-**B** sector—it is four to five time larger ($\pm$ 20–25%) than found during the daytime.

Panel (c) in Fig. 7 offers an attempt to relate the daytime and nighttime variability results for the high-**B** region on Mars to the variability of the magnetic field inclination angle (I) in that sector. As done with the TEC data, ΔI (%) was computed with respect to a control curve formed from all longitudes in the southern hemisphere outside the region of interest. As might be expected for such a broad zonally-average parameter, the mean inclination angle is near 45° everywhere, i.e., regardless of the magnitude of **B**. Thus, the percent deviations in panel (c) are positive for latitudes where the **B**-field is more vertical, and negative where it is more horizontal. Here we can see some fine-scale correlations shown by the horizontal lines drawn at specific latitudes. The clearest patterns occur in the left and central panels at four latitudes between −50 and −62° (thick horizontal lines) where peaks in nighttime variability correlate with troughs in daytime variability, and vise versa. Somewhat similar effects occur (thin horizontal lines) at the five additional latitudes of −44, −68, −72, −76 and −80°. In the right panel, the nine latitudes identified have a corresponding association with changes in **B**-field inclination patterns. At latitudes where ΔI (%) is more vertical (positive values), the nighttime ΔTEC (%) changes are positive; at latitudes where ΔI (%) is more horizontal (negative values), nighttime ΔTEC (%) changes are lowest. For daytime conditions, the ΔTEC (%) patterns at the same nine latitudes show the opposite correlations with ΔI (%). This represents the first evidence of the crustal **B**-fields exerting a clear observational consequence upon the daytime ionosphere at Mars.

To assess the reliability of the patterns shown in the top panels of Fig. 7, we are faced with the issue of characterizing the variability of variability patterns. Recalling the results from previous figures, any sample-average of TEC values results in a standard deviation (σ) of $\pm$15% for daytime TEC and $\pm$75% for nighttime TEC. The statistical certainty in reproducing a mean value is given by the error of the mean, $\sigma/(n)^{1/2}$, where n is the number of values used to form the mean (and σ). Given the large number of TEC values used to form average patterns within and beyond the region of interest, the resultant errors of the mean for panels (a) and (b) were $\sim$1% and $\sim$3%, respectively. These are less than the variations shown in panels (a) and (b). For panel (c), the overall error of the mean was $\sim$5%, and this too is smaller than the fluctuations shown. Our conclusion is that the patterns depicted in the top three panels of Fig. 7 represent reliable trends.

In panel (d) of Fig. 7, we explore further the daytime vs. nighttime TEC variability trends within the sector of strong crustal-**B** patterns in a way more directly linking ΔTEC (%) to the inclination angles. To form panel (d), we used the variability values in panels (a) and (b) for the daytime and nighttime data sets, respectively, versus the magnitude of their inclination angles between latitudes 30–85° South. While a visual trend is noticeable, the correlations are not strong statistically, with −0.20 (day) and 0.56 (night). Yet, the combination of all four panels in Fig. 7 offers incentive to explore the daytime patterns with additional years of data.

4.3. Theoretical considerations and modeling results for daytime vs. nighttime effects

Magnetic fields play many roles in ionospheric physics. Of prime interest here are the effects of **B** upon plasma dynamics—enabling plasma diffusion along crustal-**B**, inhibiting it perpendicular to

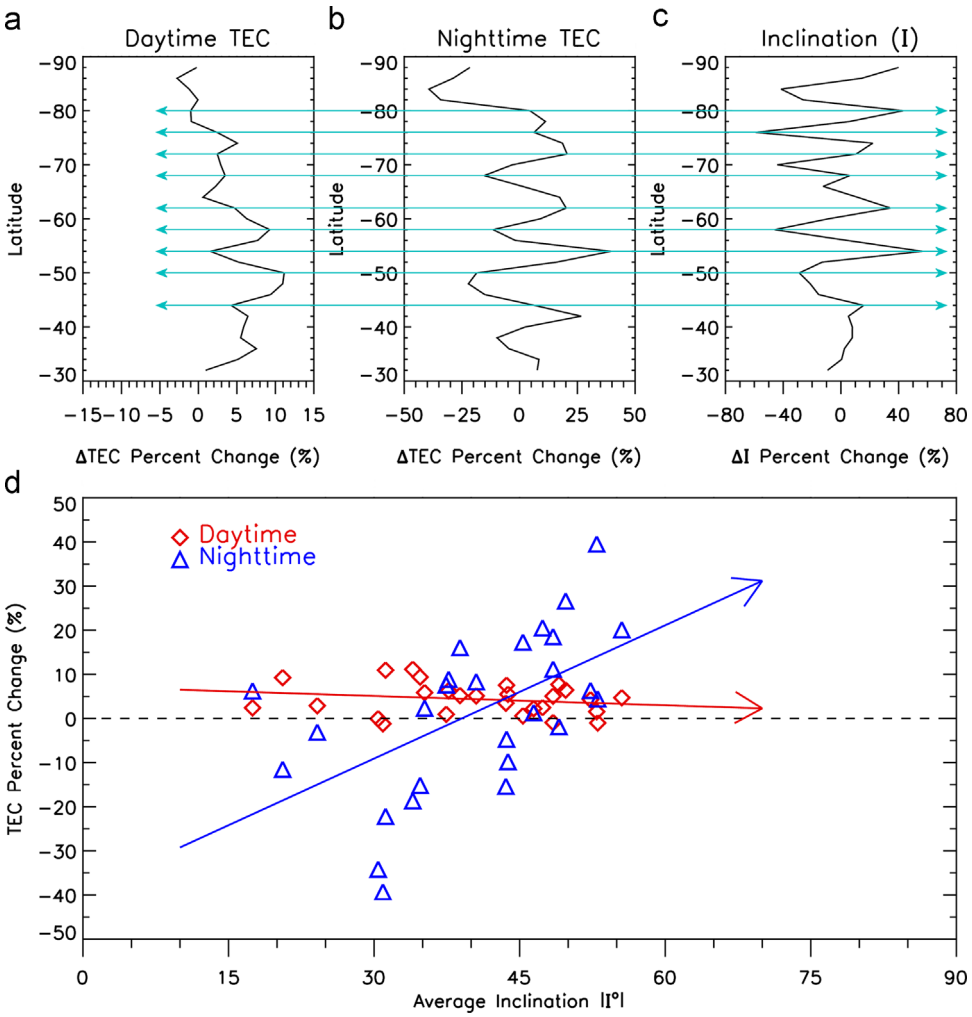

Fig. 7. Comparison of the latitude profiles (30–90°S) of ΔTEC (%) for the southern hemisphere's high-**B** longitude sector (150–210°E) with the characteristics of magnetic field inclination (*I*) variability. In panels (a) and (b), the percentage change in TEC vs. latitude was formed with respect to the zonal average of TEC at all longitudes outside the region of interest. In panel (c) the latitude profile for the percentage change in inclination angle Δ*I*(%) for the high-**B** sector, computed with respect to the mean Inclination versus latitude from all other longitudes in the southern hemisphere. The horizontal lines linking each figure occur at latitudes −44, −50, −54, −58, −62, −68, −72, −76 and −80°. See text for discussion of uncertainties. Regions of maximum correlation are shown using thicker line segments for latitudes between −50 and −62°. In panel (d), the parameters shown in panels (a) and (b) below 85°S are plotted versus the magnitude of the inclination angle (*I*), with red for daytime and blue for nighttime. See text for discussion.

crustal-**B**, and channeling horizontal transport along draped **B**-lines. It is important to realize that magnetic field topology can only affect the ionosphere at heights above the photo-chemical domain where the maximum electron density occurs. This is typically above heights of 170 to 200 km and thus of particular relevance to TEC that has a significant contribution from the topside ionosphere of Mars. Magnetic field effects upon the martian ionosphere were first treated in detail by Shinagawa and Cravens (1989). They modeled daytime conditions appropriate for the Viking lander site at low latitudes. Shinagawa and Cravens (1989) assumed (quite reasonably based on prior Venus studies) that the induced field would be horizontal (inclination angle = 0) within the daytime ionosphere at Mars. Their results showed that the presence of these **B**-fields reduced plasma densities in the topside ionosphere (due to transport effects) in comparison to the case of an ionosphere with **B** = 0 everywhere. The $N_e(h)$ profiles for these two cases – their Fig. 4 (no-**B**) vs Fig. 11 (purely horizontal-**B**) – clearly show that the TEC would be reduced in a daytime ionosphere affected by horizontal **B**-fields. The subsequent modeling by Morel et al. (2004) addressed the TEC effects quantitatively by examining the consequence of horizontal **B**-fields above 200 km. They found that the size of the reduction in TEC in a region of draped solar wind field would be about 20% (as shown in their Figs. 6 and 7). These two important modeling studies have applicabilities throughout the dayside ionosphere of Mars—independent of any influence of crustal-**B** fields.

Shinagawa and Cravens (1989) also addressed the topic of intrinsic **B**-fields, but with one major assumption that needs to be recalled—namely, that they assumed in their model a horizontal **B**-field of planetary origin. The effect of horizontal **B** was, once again, to impede vertical plasma diffusion, and thus topside densities were "slightly larger" when their intrinsic **B**-fields were stronger. This implies an enhancement of TEC above regions of horizontal-**B**, as indicated in Fig. 7. This is a positive effect quite separate from the opposite influence of solar wind draped fields upon the topside ionosphere. When the crustal-**B** longitudes are in sunlight, one might expect these two effects to interact in ways more complicated than when treated separately.

Returning to Fig. 7, and mindful of the hazards mention above of using "cusp-like" and "equatorial-like" terms in attempts to simplify complex morphology patterns over small horizontal distances, it is still tempting to associate the nighttime peaks with precipitation induced additions to TEC when *I* tends toward 90° and not so when *I* tends towards 0° (Nielsen et al., 2007). Similarly, daytime peaks in TEC above regions where *I* tends to low values

are consistent with conditions where downward diffusion of solar produced plasma (and thus to altitudes of increased chemical loss) is inhibited by horizontal **B**-fields, resulting in slightly higher TEC values. As discussed in Zou et al. (2010), an alternate way to increase electron densities at Mars is to have the electron temperatures enhanced, thereby suppressing the recombination of O_2^+ and e^- (Krymskii et al., 2003). These effects clearly warrant further study, both observationally to confirm patterns and via simulations to explore such a highly coupled photo-chemical/magnetized-plasma system.

5. Discussion

5.1. Global patterns

We have examined a two-year data set of total electron content (TEC) observations of the ionosphere of Mars obtained by the MARSIS instrument on the Mars Express satellite. The TEC parameter available for analysis was extracted as a by-product of the ionospheric corrections to radar ranging experiments (Safaeinili et al., 2003, 2007; Mouginot et al., 2008). It was anticipated that the derived TEC data would exhibit strong solar control, as indeed was the case when the same MARSIS TEC data archive was analyzed for correlations with solar zenith angle (SZA) by Safaeinili et al. (2007) and Lillis et al. (2010). In this study, we sought additional ways to portray ionospheric variability by analyzing the TEC data sorted by the geometrical parameters that lead to SZAs, i.e., latitude, season and local time. The presentations of data in the latitude vs. local time format (in Fig. 1) represent worthy targets for global diurnal modeling of the martian ionosphere. In a preliminary attempt to do so, we present in Fig. 8 a global map of TEC obtained using the 1-dimensional (vertical) Boston University Mars Ionosphere Model described in Mendillo et al. (2011). The average solar irradiance appropriate for the time span of the MARSIS observations was used (F10.7=80 units at Earth), and northern hemisphere summer solstice conditions were adopted. In the BU model, basic photo-chemistry and plasma diffusion are used to solve for $N_e(h)$ profiles. Runs were made at grid points of 5° in latitude and 1-h in local time, and the TEC was formed by integrating the model $N_e(h)$ profiles between 80 and 400 km.

In examining the model results in Fig. 8 (top panel), note that the TEC color bar used spans three decades in order to show the strong absolute magnitude differences between latitudes in continuous sunlight (northern polar regions with TEC= ~7 TECU) and the continuous nighttime conditions at high latitudes in the southern hemisphere (with TEC < 1 TECU). At the sub-solar point (24°N), the diurnal pattern reaches about 10 TECU, consistent with SZA=0° results in the Lillis et al. (2010) study. The strong temporal gradients at sunrise and sunset at mid-latitudes, as well as the pronounced daytime latitude gradient towards winter polar regions, again serve as a characteristic of a strongly solar-controlled ionosphere.

The MARSIS TEC data shown in Fig. 1 for all seasons span absolute values within two decades, the 0.1 to 10 TECU unit range ($0.1–10 \times 10^{15}$ e^-/m^2). The northern summer solstice conditions (top left panel in Fig. 1) have observations far too sparse to permit detailed comparisons. An attempt to improve this appears in the lower panel of Fig. 8. Here we have simply inverted the latitudes of the data in the central top panel of Fig. 1 so that all solstice data are averaged under the same summer–winter conditions. Moreover, we have mirrored the more abundant post-noon data into the pre-noon period (i.e., assuming photo-chemical symmetry about local noon). Finally, smoothing was done by degrading the local time resolution to 2 h. This admittedly cavalier use of data

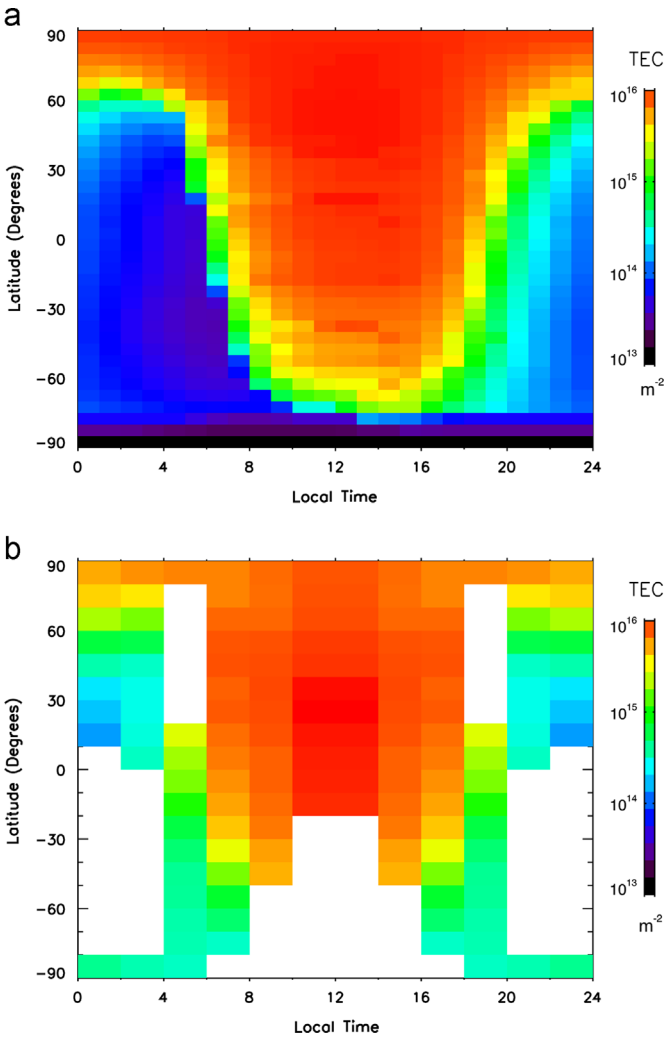

Fig. 8. (a) A global portrayal of martian total electron content (TEC) using the model described in Mendillo et al. (2011) for summer solstice conditions in the northern hemisphere. (b) MARSIS data for solstice conditions from Fig. 1, averaged under the assumption of photo-chemical symmetry (see text).

analysis (while guided by theory) points to some interesting results. First, the global pattern for northern summer solstice conditions obtained from MARSIS TEC observations exhibits a morphology broadly consistent with predictions from a basic 1-D simulation code. Over most of the planet, the observed latitude and local time gradients are comparable with model predictions. The major differences occur at high latitudes in the winter (southern) hemisphere where observed TEC is far higher than model predictions. This is probably an indicator of the important role of plasma produced by precipitation and/or horizontal transport of plasma associated with solar wind flow past the planet—processes not included in the model.

To explore model-data comparisons in a more quantitative fashion we present in Fig. 9 cross-sectional scans taken from panels (a) and (b) in Fig. 8. We do this at times when the MARSIS data are most complete. In the top panel of Fig. 9, TEC vs. latitude is shown for the mid-day period using black lines for the model and black asterisks for the observations. The 2-h LT data bin prior to noon is compared with the model run for 11:00 AM. For a data bin in late afternoon (16–18 PM), the red line and asterisks give results in comparison to the model output at 17 PM. The agreement in morphology patterns for such average conditions is acceptable.

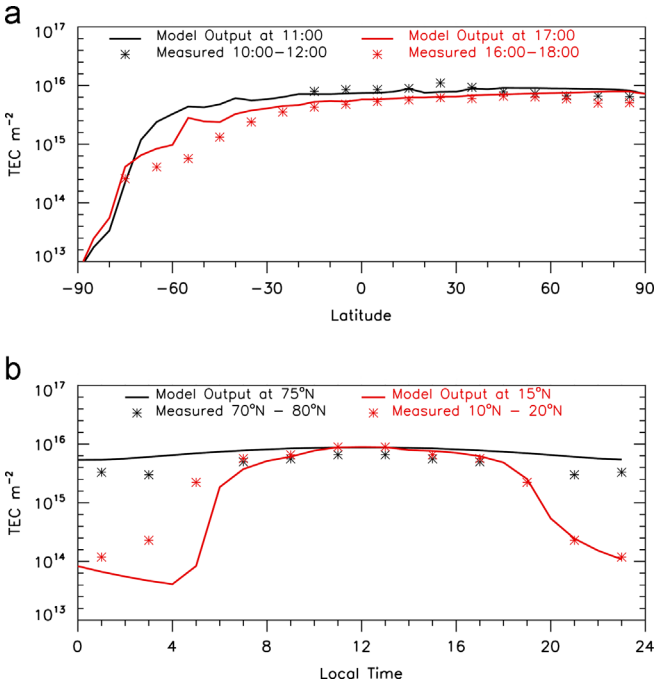

Fig. 9. Comparisons of observations with simulations taken from the results displayed in Fig. 8. (Top) TEC vs. latitude patterns at two local times: 11 AM (black curve and asterisks) and 17 PM (red curve and asterisks). (Bottom) TEC vs. local time at two latitudes: 75°N (black curve and asterisks) and 15°N (red curve and asterisks). See text.

In the lower panel of Fig. 9, we make similar comparisons for full diurnal patterns. Here the black line and asterisks give local time results at high latitudes (70–80°N), and the red curve and asterisks give local time patterns at low latitudes (10–20°N). Here the agreement is also good, except during the pre-dawn hours when the model gives somewhat lower absolute values prior to sunrise. Returning to Fig. 1 shows that observations during the midnight to noon period are simply not available (see left and center panels in the top row of Fig. 1) and thus the "MARSIS data" comes from the noon to midnight sector "reflected" patterns used to create panel (b) in Fig. 8. Thus, model-data comparisons are reasonably successful where the model's conditions best approximates the observational conditions.

5.2. *Ionospheric variability*

With confidence that the average patterns contained in the MARSIS TEC represent true morphology aspects of the martian ionosphere, we then turned to our main goal—the departures of observations from their statistical means. To study observed ionospheric variability, we focused on several analyses that used the standard deviation about the mean as a way to portray variability in a consistent manner. The conclusions reached are as follows: (1) The daytime ionosphere at Mars has a global mean variability of ~20%, and that estimate does not have a particularly strong modulation in either latitude or longitude. It is somewhat enhanced only in the 0–30° South latitude band at most longitudes, to the point that it affects the global means in that region. (2) The nighttime ionosphere at Mars has a global mean variability of ~75%, and it too does not have latitude or longitude regions that dominate the global mean pattern. Nighttime variability is locally higher in the southern hemisphere at longitudes where crustal magnetic fields are found, but the confinement in longitude of such effects gets averaged out when all longitudes are used to create a global mean variability. (3) When subjected to detailed regional analysis, however, the sector of Mars with strong crustal-**B** fields does show a significant correlation with the latitude patterns of the inclination angles of the magnetic fields. While such effects were known from previous studies of nighttime data, we have quantified the specifics of ΔTEC(%) vs. ΔI(%) and the magnitude of I for the first time. Moreover, we presented evidence that a reverse correlation may exist for daytime observations of TEC in crustal-**B** regions. Such findings reinforce the modeling conclusions reached earlier by Shinagawa and Cravens (1989) and Morel et al. (2004) that ionospheric processes will be affected wherever the magnetic field magnitude (whether crustal or induced) is high enough to do so, that is, to compete with the non-electrodynamical, photo-chemical and diffusive conditions in the ambient ionosphere.

Finally, attempts to model ionospheric variability at Mars have only been conducted in a single study to date. Martinis et al. (2003) presented the first simulation of day-to-day variability of electron density profiles at Mars obtained by the Mars Global Surveyor radio occultation experiment. Their study was focused only on the contribution to variability caused by daily changes in the solar irradiance spanning 17 days in March 1999. Using the same neutral atmosphere for each day in order to isolate the effects of solar flux variability, Martinis et al. (2003) found that the variability of the peak electron density (NmM2) was ~5%, while that of the minor layer (NmM1) was about 20%. This is consistent with the terrestrial case where Moore et al. (2006) found the mid-day variability to be 5–7% for the photo-chemical E-layer (the terrestrial layer most analogous to the M2-layer at Mars). Given that the martian TEC is dominated by contributions from the M2-layer and above, TEC variability induced by solar photon variability is probably higher, perhaps ~10%. This is about half of the overall observed variability shown in Fig. 4, and thus other drivers ranging from hourly to day-to-day need to be examined (Morel et al., 2004). As pointed out by Haider et al. (2011) in their Figs. 22 and 23, observed variability at the peak and in topside ionosphere exceed expectations from photo-chemical processes acting alone. Future modeling studies need to address the simultaneous changes in the neutral atmosphere that would accompany solar variability. The role of winds needs to be assessed, both for horizontal plasma transport in regions of weak **B**-fields as well as for field-aligned transport where **B**-fields are strong. Atmospheric gravity waves and tides will also contribute to ionospheric variability, and perhaps more so in regions where topographic variability is significant. Finally, the major driver of variability in TEC (recalling that 2/3rd of it is in the topside ionosphere) may well be the ever-changing influence of the solar wind upon the martian topside ionosphere. Morel et al. (2004) have shown that the N_e(h) contributions above 200 km can change the overall TEC by ~20% for cases with and without solar wind draping. Such models that have treated steady-state solar wind effects need to be expanded to address ionospheric variability driven by day-to-day changes in the solar wind.

Acknowledgements

At Boston University, this work was supported by grants from the following NASA programs (MDAP #NNX12AJ39G, MFRP #NNX08AN56G, LWSTRT #NNX08AP96G, P. Withers, PI), and by the comparative ionospheres component of NSF Aeronomy Program grant #AGS-1123222 (M. Mendillo, PI). The authors gratefully acknowledge G. Picardi (Universita di Roma' La Sapienza', Rome, Italy), R. Orosei, and J. Plaut, as well as the European Space Agency, for making the MARSIS data available.

References

Acuña, M.H., et al., 1998. Magnetic field and plasma observations at Mars: initial results of the Mars Global Surveyor Mission. Science 279, 1676–1680.

Arkani-Hamed, J., A coherent model of the crustal magnetic field of Mars, Journal of Geophysical Research, 109, E09005, 10.1029/JE002265 2004.

Breus, T., Krymskii, A., Crider, D., Ness, N., Hinson, D., Barashyan, K., 2004. Effect of the solar radiation in the topside atmosphere/ionosphere of Mars: Mars Global Surveyor observations. Journal of Geophysical Research 109, http://dx.doi.org/10.1029/2004JA010431.

Bust, G., Mitchell, C., 2008. History, current state, and future directions of ionospheric imaging. Reviews of Geophysics 46, RG1003, http://dx.doi.org/10.1029/RG000212.

Cartacci, M., Amata, E., Cicchetti, A., Noschese, R., Giuppi, S., Langlais, B., Frigeri, A., Orosei, r., Picardi, G., 2013. Mars ionosphere total electron content analysis from MARSIS subsurface data. Icarus. (in press).

Chacko, C., Mendillo, M., 1977. Electron density enhancements in the F region beneath the magnetospheric cusp. Journal of Geophysical Research 82, 4757–4764.

Connerney, J., Acuña, M., Wasilewski, P., Kletetschka, G., Ness, N., Rème, H., Lin, R., Mitchell, D., 2001. The global magnetic field of Mars and implications for crustal evolution. Geophysical Research Letters 28 (21), 4014–4018, http://dx.doi.org/10.1029/2001GL013619.

Creasey, J., Forbes, J., 2006. Global and seasonal distribution of gravity wave activity in Mars' lower atmosphere derived from MGS radio occultation data. Geophysical Research Letters 33, L01803, http://dxdoi.org/10.1029/2005GL024037.

Duru, F., Gurnett, D., Averkamp, T., Kirchner, D., Huff, R., Persoon, A., Plaut, J., Picardi, G., 2006. Magnetically controlled structures in the ionosphere of Mars. Journal of Geophysical Research 111, A12204, http://dx.doi.org/10.1029/2006JA011975.

Forbes, J., Palo, S., Zhang, S.-E., 2000. Variability of the ionosphere. Journal of Atmospheric and Solar-Terrestrial Physics 62, 685–693.

Fox, M., Mendillo, M., Klobuchar, J., 1991. Ionospheric equivalent slab thickness and its modeling applications. Radio Science 26 (2), 429–438.

Fox, J., K. Yeager, Morphology of the near-terminator Martian ionosphere: a comparison of models and data, Journal of Geophysical Research, 111, 10.1029/JA011697 2006.

Gurnett, D.A., et al., 2005. Radar sounding of the ionosphere of Mars. Science 310, 1929–1933, http://dx.doi.org/10.1126/science.1121868.

Haider, S., Mahajan, K., Kallio, E., 2011. Mars ionosphere: a review of experimental results and modeling studies. Reviews of Geophysics 49, RG4001, http://dx.doi.org/10.1029/2011RG000357.

Kelley, M., 2009. The Earth's Ionosphere: Plasma Physics and Electrodynamics, second ed. Academic Press, Elsevier Pub., Amsterdam.

Krymskii, A., Breus, T., Ness, N., Hinson, D., Bojkov, d., 2003. Effect of crustal magnetic fields on the near terminator ionosphere at Mars: comparison of in situ magnetic field measurements with the data of radio science experiments on board Mars Global Surveyor. Journal of Geophysical Research 108, http://dx.doi.org/10.1029/2002JA009662.

Krymskii, A.M., et al., 2004. Solar wind interaction with the ionosphere/atmosphere and crustal magnetic fields at Mars: Mars Global Surveyor magnetometer/electron reflectometer, radio science, and accelerometer data. Journal of Geophysical Research 109, A11306, http://dx.doi.org/10.1029/2004JA010420.

Lillis, R., Brain, D., England, S., Withers, P., Fillingim, M., Safaeinili, A., 2010. Total electron content in the Mars ionosphere: temporal studies and dependence on solar EUV flux. Journal of Geophysical Research , http://dx.doi.org/10.1029/2010JA015698.

Martinis, C., Wilson, J., Mendillo, M., 2003. Modeling day-to-day ionospheric variability on Mars. Journal of Geophysical Research 108 (A10), 1383 http://dx.doi.org/10.1029/2003JA009973.

Mendillo, M., 2006. Storms in the ionosphere: patterns and processes for total electron content. Reviews of Geophysics 44, RG4001, http://dx.doi.org/10.1029/2005RG000193.

Mendillo, M., Chacko, C., 1977. The base level ionospheric trough. Journal of Geophysical Research 82, 5129–5137.

Mendillo, M., Withers, P., 2008. Solar flare effects upon the ionospheres of Earth and Mars. In: Song, P., Foster, J., Mendillo, M., Bilitza, D. (Eds.), Radio Sounding and Plasma Physics. American Institute of Physics, New York. (#CP974 (978-0-7354-0493-9/08).

Mendillo, M., Lollo, A., Withers, P., Matta, M., Patzold, M., Tellmann, S., 2011. Modeling Mars' ionosphere with constraints from same-day observations by Mars Global Surveyor and Mars Express. Journal of Geophysical Research 116, A11303, http://dx.doi.org/10.1029/2011JA016865.

Mendillo, M., Smith, S., Wroten, J., Rishbeth, H., 2003. Simultaneous ionospheric variability on Earth and Mars. Journal of Geophysical Research 108 (A12), 1432, http://dx.doi.org/10.1029/JA00996.

Mendillo, M., Pi, X.-Q., Smith, S., Martinis, C., Wilson, J., Hinson, D., 2004. Ionospheric effects upon a satellite navigation system at Mars. Radio Science 39, RS2028, http://dx.doi.org/10.1029/2003RS002933.

Mendillo, M., Withers, P., Hinson, D., Rishbeth, H., Reinisch, B., 2006. Effects of solar flares on the ionosphere of Mars. Science 311, 1135–1138, http://dx.doi.org/10.1126/science.1122099.

Moore, L., Mendillo, M., Martinis, C., Bailey, S., 2006. Day-to-day variability of the E layer. Journal of Geophysical Research 111, A06307, http://dx.doi.org/10.1029/2005JA011448.

Morel, L., Witasse, O., Warnant, R., Cerisier, J.-C., Blelly, P.-L., Lilensten, J., 2004. Diagnostic of the dayside ionosphere of Mars using the total electron content measurement by the NEIGE/Netlander experiment: an assessment study. Planetary and Space Science 52, 603–611.

Mouginot, J., Kofman, W., Safaeinili, A., Herique, A., 2008. Correction of the ionospheric distortion on the MARSIS surface sounding echoes. Planetary and Space Science 56, 917–926.

Nagy, A., et al., The plasma environment of Mars, Space Science Reviews, 111, 33-114, 10.1023/B:SPAC.0000032718.47512.92 2004.

Němec, F., Morgan, D., Gurnett, D., Brain, D., 2011. Areas of enhanced ionization in the deep nightside ionosphere of Mars. Journal of Geophysical Research 116, E06006, http://dx.doi.org/10.1029/JE003804.

Němec, F., Morgan, D., Gurnett, D., Dunn, F., 2010. Nightside ionosphere of Mars: radar soundings by the Mars Express spacecraft. Journal of Geophysical Research 115, E12009, http://dx.doi.org/10.1029/2010JE003663.

Nielsen, E., 2007. 13 co-authors, 2007. Local plasma processes and enhanced electron densities in the lower ionosphere in magnetic cusp regions on Mars. Planetary and Space Science 55, 2164–2172.

Pandya, B., Haider, S., 2012. Meteor impact perturbations in the lower ionosphere of Mars: MGS observations. Planetary and Space Science 63, 105–109, http://dx.doi.org/10.1016/j.pss.2011.089.013.

Pätzold, M., Tellmann, S., Häusler, B., Hinson, D., Schaa, R., Tyler, G., 2005. A sporadic third layer in the ionosphere of Mars. Science 310, 837–839 http://dx.doi.org/10.1126/science.1117755.

Picardi, G., et al., 2005. Radar soundings of the subsurface of Mars. Science 310 (5756), 1925–1928, http://dx.doi.org/10.1126/science.1122165.

Rishbeth, H., Garriott, O.K., 1969. Introduction to Ionospheric Physics. Academic Press, New York.

Rishbeth, H., Mendillo, M., 2001. Patterns of F2-layer variability. Journal of Atmospheric and Solar-Terrestrial Physics 63, 1661–1680.

Safaeinili, A., Kofman, W., Mouginot, J., Gim, Y., Herique, A., Ivanov, A., Plaut, J., Picardi, G., 2007. Estimation of the total electron content of the Martian ionosphere using radar sounder surface echoes. Geophysical Research Letters 34, L23204, http://dx.doi.org/10.1029/2007GL032154.

Safaeinili, A., Kofman, W., Nouvel, J.-F., Herique, A., Jordan, R., 2003. Impact of Mars ionosphere on orbital radar sounder operation and data processing. Planetary and Space Science 51, 505–515, http://dx.doi.org/10.1016/S0032-0633(03)00048-5.

Schunk, R., Nagy, A., 2009. Ionospheres: Physics, Plasma Physics, and Chemistry, second ed. Cambridge University Press.

Shinagawa, H., Cravens, T., 1989. A one-dimensional multispecies magnetohydrodynamic model of the dayside ionosphere of Mars. Journal of Geophysical Research 94 (A6), 6506–6516.

Titheridge, J., 1973. The slab thickness of the ionosphere. Planetary and Space Science 21, 1775–1793.

Withers, P., 2009. A review of observed variability in the dayside ionosphere of Mars. Advances in Space Research 44, 277–307, http://dx.doi.org/10.1016/j.asr.2009.04.027.

Withers, P., Mendillo, M., Hinson, D., Cahoy, K., 2008. Physical characteristics and occurrence rates of meteoric plasma layers detected in the Martian ionosphere by the Mars Global Surveyor Radio Science Experiment. Journal of Geophysical Research 113, http://dx.doi.org/10.1029/JA013636.

Withers, P., Mendillo, M, Rishbeth, H., Hinson, D., Arkani-Hamed, J., 2005. Ionospheric characteristics above Martian crustal magnetic anomalies. Geophysical Research Letters 32, L16204, http://dx.doi.org/10.1029/2005GL023483.

Wright, J.W., 1960. A model of the F region above h_{max}F2. Journal of Geophysical Research 65 (1), 185–191, http://dx.doi.org/10.1029/JZ065i001p00185.

Zou, H., Chen, H.-F., Yu, N., Shi, W.-H., Yu, X.-Q., Zou, J.-Q., Zhong, W.-Y., 2010. Effects of Martian crustal field on its ionosphere. Science China Technological Sciences 53, 1717–1724, http://dx.doi.org/10.1007/s11431-010-3118-1.